Carbohydrate Polymers 98 (2013) 1072–1082

Contents lists available at SciVerse ScienceDirect

Carbohydrate Polymers

journal homepage: www.elsevier.com/locate/carbpol

High-barrier coated bacterial cellulose nanowhiskers films with reduced moisture sensitivity

Marta Martínez-Sanz, Amparo Lopez-Rubio, Jose M. Lagaron*

Novel Materials and Nanotechnology Group, IATA, CSIC, Avda. Agustín Escardino, 7, 46980 Paterna, Valencia, Spain

ARTICLE INFO

Article history:
Received 5 February 2013
Received in revised form 27 June 2013
Accepted 9 July 2013
Available online 17 July 2013

Keywords:
Bacterial cellulose
Nanowhiskers
Polylactide
Silanes
Electrospinning
Barrier properties

ABSTRACT

This study reports on the development and characterization of bacterial cellulose (BCNW) films coated with hydrophobic layers, presenting enhanced barrier properties. Pure BCNW films showed good transparency and thermal stability, high rigidity and extremely low oxygen permeability at 0%RH. The dramatic increase in oxygen permeability at 80%RH, due to the hydrophilic character of BCNW, was counteracted through coating the films with annealed PLA electrospun nanostructured fibres or hydrophobic silanes. The use of electrospinning was crucial to attain a good adhesion between the hydrophilic BCNW and the hydrophobic PLA layer. After electrospinning, the fibres were homogenised by annealing, thus obtaining a uniform and continuous coating. Coated systems showed a hydrophobic surface and protected the BCNW from moisture, thus reducing ca. 70% the water permeability and up to 97% the oxygen permeability at 80%RH. Furthermore, this novel approach was seen to protect BCNW films from moisture more efficiently than coating with hydrophobic silanes.

1. Introduction

Cellulose is the most abundant biopolymer found in nature, as it is the major cell-wall component of plants. Although cellulose is commonly extracted from vegetal resources, some bacterial species are able to produce bacterial cellulose (BC) as a highly hydrated pellicle which, compared to plant cellulose, possesses higher water holding capacity, higher crystallinity and a finer web-like network (Iguchi, Yamanaka, & Budhiono, 2000; Wan et al., 2007). Furthermore, one of the main advantages of BC is that, while cellulose derived from plants is naturally associated with other biopolymers such as hemicellulose and lignin, BC is predominantly pure cellulose and, thus, no additional processes are needed in order to isolate cellulose.

For their application as nanofillers, cellulosic materials are usually subjected to hydrolysis with strong acids, which produce a preferential digestion of the amorphous domains of the material and cleavage of the nanofibril bundles (Rånby, 1949), breaking down the hierarchical structure of the material into nanocrystals, which are usually referred to as cellulose nanowhiskers (CNW). Bacterial cellulose nanowhiskers (BCNW) present a highly crystalline structure (Martínez-Sanz, Lopez-Rubio, & Lagaron, 2011a), with up to several micrometres in length and a cross-section of 5–50 nm (De Souza Lima & Borsali, 2004; Hirai, Inui, Horii, & Tsuji, 2009).

Due to their attractive properties, such as low density and biodegradability, great interest has been focused lately on the use of cellulose nanocrystals as reinforcing agents in nanocomposites (Kvien, Sugiyama, Votrubec, & Oksman, 2007; Martínez-Sanz, Lopez-Rubio, & Lagaron, 2012b,d; Petersson, Kvien, & Oksman, 2007; Ten, Turtle, Bahr, Jiang, & Wolcott, 2010), although due to their highly hydrophilic character, which is responsible for their incompatibility with organic solvents and for their poor adhesion to the hydrophobic surface of conventional polymeric materials, strategies have to be developed in order to guarantee a proper dispersion of cellulosic nanofillers in polymeric nanocomposites.

In addition to their application as reinforcing agents in nanocomposites, pure cellulose films may be produced from cellulose nanocrystals and microfibrillated cellulose aqueous suspensions via solution casting (Aulin, Gällstedt, & Lindström, 2010; Belbekhouche et al., 2011; Fukuzumi, Saito, Iwata, Kumamoto, & Isogai, 2009; Minelli et al., 2010; Plackett et al., 2010; Rodionova et al., 2011; Siró, Plackett, Hedenqvist, Ankerfors, & Lindström, 2011; Syverud & Stenius, 2009). These films show excellent oxygen barrier properties at low relative humidity due to their high crystallinity and highly compacted structure (Belbekhouche et al., 2011; Minelli et al., 2010; Plackett et al., 2010; Syverud & Stenius, 2009). It has been reported that the denser structure and the formation of entanglements in films prepared from microfibrillated cellulose gives rise to increased barrier to gases as compared to cellulose nanowhiskers' films (Belbekhouche et al., 2011).

* Corresponding author. Tel.: +34 963900022; fax: +34 963636301.
E-mail address: lagaron@iata.csic.es (J.M. Lagaron).

0144-8617/$ – see front matter © 2013 Elsevier Ltd. All rights reserved.
http://dx.doi.org/10.1016/j.carbpol.2013.07.020

Despite the outstanding barrier properties of cellulose films at low relative humidity, they present a typical behaviour of hydrophilic materials, i.e. the permeability increases sharply in the range of 40–80% relative humidity (Aulin et al., 2010). This exponential increase on the oxygen permeability when increasing the relative humidity has been attributed to the fact that water molecules adsorbed by the amorphous domains of cellulose may break down hydrogen bonds and, therefore, preferential sites for oxygen diffusion are created (Aulin et al., 2010). In order to reduce the hydrophilicity of cellulose and restrict the detrimental effect of humidity in its properties, hydrophobization of the cellulose surface has been proposed. TEMPO-oxidized cellulose nanofibres' films produced via vacuum filtration, displaying good mechanical properties and high barrier to oxygen at 0%RH, were effectively hydrophobized by treatment with alkylketene dimer although no barrier properties were reported for the hydrophobized films (Fukuzumi et al., 2009). In another study, acetylation of microfibrillated cellulose was successfully developed and films from modified cellulose were produced (Rodionova et al., 2011). Although the surface of the films became hydrophobic, it was observed that the substitution of hydroxyl groups led to increased pore volume in the films due to reduced hydrogen bonding between cellulose microfibrils. Thus, only acetylated cellulose films with a low degree of OH substitution presented improved water vapour permeability as compared to unmodified cellulose films. A similar effect was observed for films produced from silylated microfibrillated cellulose. When high degrees of OH substitution were achieved, the so-obtained films displayed contact angles typical of super hydrophobic surfaces. However, partial solubilization of cellulose microfibrils was seen to occur for high degrees of substitution (Andresen, Johansson, Tanem, & Stenius, 2006).

In the present study, highly crystalline BCNW were used to produce films with excellent barrier properties at low relative humidity. Given the high rigidity of the BCNW films, the addition of PEG as plasticizing agent was additionally evaluated. As a strategy for preserving the high barrier of BCNW films under high relative humidity conditions without the need for a previous chemical modification of the cellulose matrix, BCNW films were coated with PLA by a novel method consisting in deposition of fibres by electrospinning followed by homogenization through annealing. Additionally, this approach was compared with a more conventional method which involved the application of hydrophobic silanes layers.

2. Materials and methods

2.1. Materials

The semicrystalline polylactide (PLA) used was a film extrusion grade produced by Natureworks (with a D-isomer content of approximately 2%). The molecular weight had a number-average molecular weight (M_n) of ca. 130,000 g/mol, and the weight average molecular weight (M_w) was ca. 150,000 g/mol as reported by the manufacturer.

Vinyltrimethoxysilane (VTMS) and (3-aminopropyl) trimethoxysilane (APTS) were purchased from Sigma-Aldrich (Germany).

Sulphuric acid 96% and 2-propanol were purchased from Panreac (Barcelona, Spain). Both 1,1,1,3,3,3-hexafluoro-2-propanol (HFP) and polyethylene glycol 900 (PEG) were purchased from Fluka (Germany).

2.2. Preparation of bacterial cellulose mats

Bacterial cellulose mats were obtained by following the same procedure as described in a previous work (Martínez-Sanz, Olsson, Lopez-Rubio, & Lagaron, 2011b). Briefly, the bacterial strain *Gluconacetobacter xylinus* 7351 was incubated in a modified Hestrin/Shramm medium at 30 °C. All of the cells were pre-cultured in a test tube containing 5 mL of media and later transferred and scaled up to a bigger reactor of 20 L. The synthesized bacterial cellulose pellicles were sterilized and cleaned in boiling water and in a 10% (v/v) NaOH aqueous solution.

2.3. Preparation of bacterial cellulose nanowhiskers (BCNW)

Once neutral pH was reached, bacterial cellulose pellicles were ground in a blender and the gel-like material was then compressed in order to remove most of the absorbed water. BCNW were produced by applying the optimized method developed in a previous study (Martínez-Sanz et al., 2011a). Briefly, the dried bacterial cellulose was treated with 301 mL sulphuric acid/L water, in a cellulose/acid ratio of approximately 7 g/L, at 50 °C for three days until a homogeneous solution was obtained. The cellulose nanowhiskers were obtained as a white precipitate after several centrifugation and washing cycles at 12,500 rpm and 15 °C for 20 min. After that, the material was re-suspended in deionized water and neutralized with sodium hydroxide until neutral pH and subsequently centrifuged to obtain the final product as a partially hydrated precipitate. The humidity of the material was determined and the yield of the extraction process was estimated to be 79.64% respect to the dried BC.

2.4. Preparation of BCNW films

Bacterial cellulose nanowhiskers films were produced from aqueous suspensions of BCNW 0.5% (w/v). These suspensions were prepared by dispersing the adequate amount of partially hydrated precipitate into 50 mL of deionized water by means of intense homogenization (Ultra-turrax) for 2 min and sonication for 5 min. Additional samples were prepared by adding 20 wt% polyethylene glycol (PEG) and dispersing it together with the BCNW. The BCNW/water or BCNW–PEG/water dispersions were subjected to vacuum filtration through a polytetrafluoroethylene (PTFE) membrane with a 0.2 μm pore size (Sartorius Stedim Biotech GmbH, Germany). After filtration, the material was dried at ambient temperature overnight and BCNW or BCNW–PEG films were then peeled off from the PTFE membranes.

2.5. Preparation of coated systems

In order to protect the highly hydrophilic BCNWs' layer, several methods were tested for coating with hydrophobic materials.

The first method consisted in coating the BCNW or BCNW–PEG films with PLA mats produced by means of the electrospinning technique. PLA solutions in HFP having a total solids content of 8 wt% were used to generate the electrospun fibres. An electrospinning apparatus a Fluidnatek equipment from Bioincia S.L., Paterna (Spain) was used. Solutions were transferred to 5 mL plastic syringes and connected through PTFE tubes to a stainless steel needle (⌀ 0.9 mm). An electrode was clamped to the needle tip and connected to a high-voltage 0–30 kV power supply operating at 10–12 kV, and the polymer solution was fed into the needle at a rate of 0.66 mL/h by a syringe pump. The counter electrode was connected to a circular plate in which the BCNW film was attached. The plate was placed parallel to the needle and both sides of the BCNW film were coated. The distance between the needle and the plate was 6 cm and experiments were carried out at ambient temperature. By applying this procedure, BCNW and BCNW–PEG films were coated with 40–50 wt% PLA electrospun fibres.

Electrospun PLA coatings presented an opaque and whitish appearance. With the aim of obtaining a transparent and

continuous pellicle, an additional heating step was applied. Coated films were first dried at 60 °C overnight, and they were subsequently placed in between hot plates at 160 °C to melt and homogenize the PLA phase.

The second method involved the hydrophobization of the films surface by coating with layers of two different silanes. Both vinyltrimethoxysilane (VTMS) and (3-aminopropyl) trimethoxysilane (APTS) are suitable for food contact applications. The methoxy functionalities are able to react with the hydroxyl groups of cellulose, thus being possible to produce silane coatings. The liquid silanes were applied on both sides of BCNW films by using a paint roller. Subsequently, films were dried under ambient conditions during 10 mins and then cured at 60 °C for 48 h.

2.6. Scanning electron microscopy (SEM)

SEM was conducted on a Hitachi microscope (Hitachi S-4100) at an accelerating voltage of 10 kV and a working distance of 12–16 mm. BCNW and BCNW–PEG films as well as the coated systems were cryo-fractured after immersion in liquid nitrogen and subsequently sputtered with a gold–palladium mixture under vacuum before their morphology was examined using SEM. Layer thicknesses were measured by means of the Adobe Photoshop CS3 extended software from the SEM micrographs in their original magnification.

2.7. Attenuated total reflectance (ATR) FT-IR analysis

ATR-FTIR spectra of all the produced films were recorded in a controlled chamber at 21 °C and 40%RH using a Bruker (Rheinstetten, Germany) FT-IR Tensor 37 equipment and coupling the ATR accessory GoldenGate of Specac Ltd. (Orpington, UK). The spectra were taken at 4 cm^{-1} resolution averaging a minimum of 20 scans. Analysis of the spectra was performed using Grams/AI 7.02 (Galactic Industries, Salem, NH, USA) software.

2.8. Thermogravimetric analysis (TGA)

Thermogravimetric (TG) curves were recorded with a TA Instruments model Q500 TGA. The samples (ca. 20 mg) were heated from 50 °C to 600 °C with a heating rate of 10 °C/min under nitrogen atmosphere. Derivative TG curves (DTG) express the weight loss rate as a function of temperature.

2.9. Mechanical properties

Tensile tests were carried out under ambient conditions typically at 24 °C and 50%RH on an Instron 4400 Universal Tester. Pre-conditioned dumb-bell shaped specimens with initial gauge length of 25 mm and 5 mm in width were die-stamped from the films in the machine direction according to the ASTM D638. A fixed crosshead rate of 10 mm/min was utilized in all cases and results were taken as the average of, at least, four tests.

2.10. Water vapour permeability (WVP)

Direct permeability to water was determined from the slope of the weight gain versus time curves at 24 °C. The films were sandwiched between the aluminium top (open O-ring) and bottom (deposit for the silica gel that provides 0%RH) parts of a specifically designed permeability cell with screws. A Viton rubber O-ring was placed between the film and the bottom part of the cell to enhance sealability. These permeability cells containing silica gel were then placed inside a desiccator at 75%RH and the solvent weight gain through a film area of 0.001 m^2 was monitored and plotted as a function of time. The samples were preconditioned at the testing conditions for 24 h, and to estimate the permeability values of the films, only the linear part of the weight gain data was used to ensure sample steady-state conditions. Cells with aluminium films (with thickness of ca. 11 μm) were used as control samples to estimate solvent gain through the sealing. The lower limit of WVP detection of the permeation cells was of ca. 4.2×10^{-17} kg m/s m^2 Pa based on the weight gain measurements of the aluminium films. Solvent permeation rates were estimated from the steady-state permeation slopes. Water vapour weight gain was calculated as the total cell weight gain minus the gain through the sealing. The tests were done in duplicate.

2.11. Water uptake

The water uptake was estimated during the sorption experiments at 24 °C and 75% RH by means of weight gain using an analytical balance Voyager® V11140. Thus, at saturation conditions, no changes in successive weight uptake were observed during the measurements of the specimens.

Solubility (S), required to estimate the diffusion coefficient of water (D) through the films, was estimated from the water uptake at equilibrium, the density of the materials and the water vapour partial pressure at 24 °C.

2.12. Oxygen permeability

The oxygen permeability coefficient was derived from oxygen transmission rate (OTR) measurements recorded using an Oxtran 100 equipment (Modern Control Inc., Minneapolis, MN, US). Experiments were carried out at 24 °C and at two relative humidities (0%RH and 80%RH). An 80% relative humidity was generated by a built-in gas bubbler and was checked with a hygrometer placed at the exit of the detector. The samples were purged with nitrogen for a minimum of 20 h in the humidity equilibrated samples, prior to exposure to an oxygen flow of 10 mL/min. A 5 cm^2 sample area was measured by using an in-house developed mask. Reduced sample areas while testing oxygen permeation in high permeable materials enhance the reproducibility of the measurements, permit to select defect-free areas and ensure minimum thickness variations.

2.13. Contact angle measurements

Measurements of contact angle were performed at 24 °C and ambient relative humidity (ca. 60%RH) in a Video-Based Contact Angle Meter model OCA 20 (DataPhysics Instruments GmbH, Filderstadt, Germany). Contact angle measurements were obtained by analyzing the shape of a distilled water drop after it had been placed over the film for 30 s. Image analyses were carried out by SCA20 software.

3. Results and discussion

3.1. BCNW films characterization

Crystalline cellulose nanowhiskers have been extensively used as reinforcing agents in nanocomposite materials. Previous works have investigated the effect of incorporating cellulose nanowhiskers on the barrier properties of nanocomposite materials, showing significant improvements provided that a high dispersion of the nanowhiskers was achieved (Martínez-Sanz, Lopez-Rubio, & Lagaron, 2012b,c,d). In addition, microfibrillated cellulose and cellulose nanowhiskers films have shown excellent barrier properties at low relative humidity (Belbekhouche et al., 2011; Minelli et al., 2010; Siró et al., 2011). The purpose of this work was to develop high barrier materials by using highly crystalline bacterial cellulose nanowhiskers' films and to enhance the

performance of these materials at high relative humidity by coating them with hydrophobic layers.

The BCNW used in the present work were extracted by acid hydrolysis of bacterial cellulose pellicles and showed a crystallinity index of ca. 95%, as previously estimated by X-ray diffraction (Martínez-Sanz et al., 2011a). The morphology of BCNW produced by sulphuric acid hydrolysis has already been studied and, in a previous work, it was shown that BCNW extracted using the optimized hydrolysis conditions applied in the present work presented an average cross-section (W) of ca. 18 nm and length (L) of ca. 570 nm having, thus, an aspect ratio (L/W) of ca. 30 (Martínez-Sanz et al., 2011a).

Pure BCNW films presented a highly compacted nanofibres' layered structure, as shown in Fig. 1A. The material presented a highly dense structure, which was held by the strong hydrogen network established between the hydroxyl groups present on the cellulose chains, and no pores could be detected at the applied magnification. Fig. 1B shows that when incorporating the polyethylene glycol (PEG) as plasticizing agent into the films, a less-compacted structure was attained, in which PEG rich domains could be clearly discerned.

Thermal stability of BCNW and BCNW–PEG films was evaluated by TGA (see Fig. S1 in the Supporting information). The onset degradation temperature and the maximum degradation temperature for the BCNW film were determined to be 206.7 °C and 332.1 °C, respectively, which are very similar to the parameters previously reported for BCNW produced by the same optimized hydrolysis treatment (Martínez-Sanz et al., 2011a). On the other hand, the film containing PEG presented a wider degradation range, with a lower onset degradation temperature of 174.0 °C and a higher maximum degradation temperature of 342.3 °C. Therefore, it is confirmed that BCNW films can be subjected to temperatures typical for polymeric materials processing methods without suffering thermal degradation. Nevertheless, films containing PEG presented an onset degradation temperature which was close to the temperature at which films were processed.

Table 1 gathers the mechanical properties of BCNW and BCNW–PEG films. As deduced from the table, pure BCNW films displayed a rigid and brittle behaviour, with a higher Young's modulus than that previously reported for MFC films but lower elongation at break. The higher crystallinity of BCNW as compared to MFC may be the reason for this higher rigidity and reduced ductility. With the

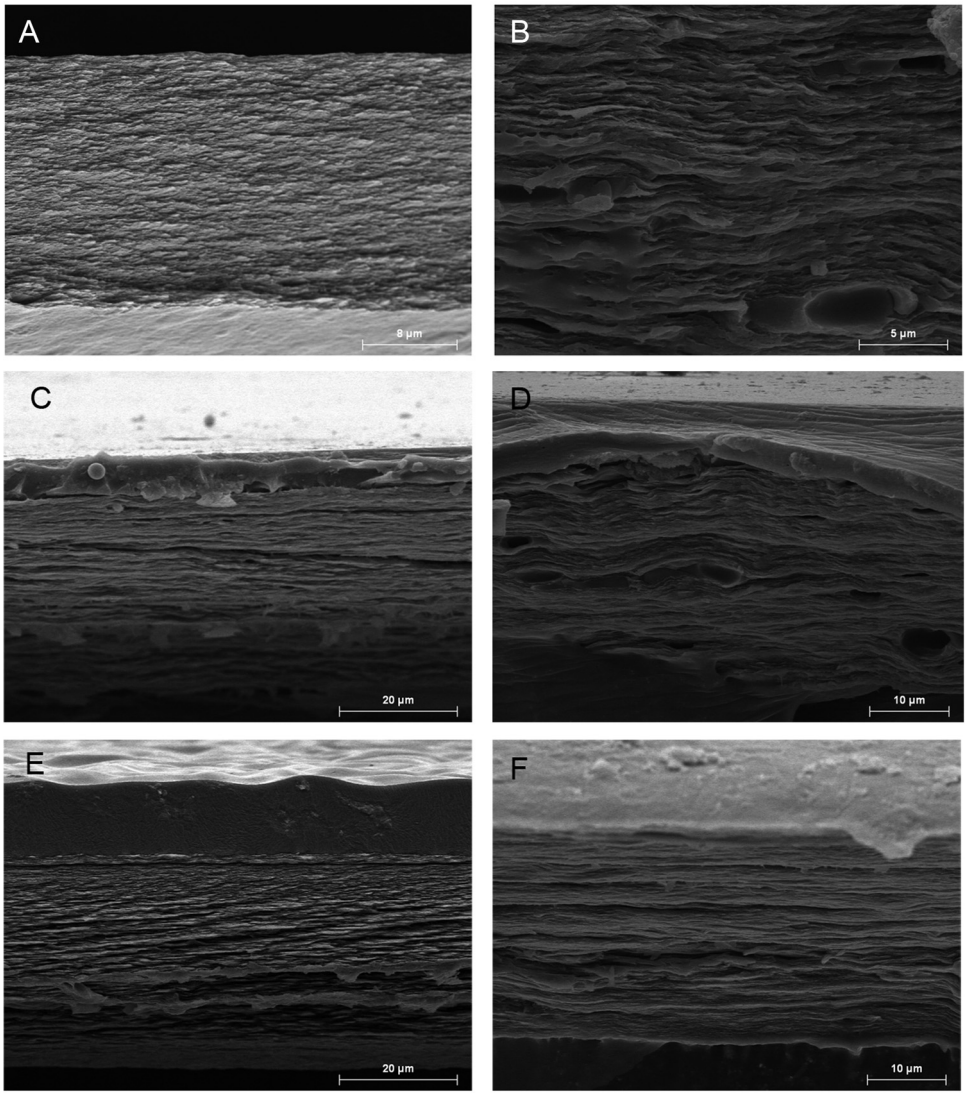

Fig. 1. SEM micrograph of cryo-fractured surfaces from: (A) BCNW film; (B) BCNW–PEG film; (C) BCNW film coated with annealed PLA electrospun nanostructured fibres; (D) BCNW film coated with annealed PLA electrospun nanostructured fibres; (E) BCNW film coated with APTS and (F) BCNW film coated with VTMS. Scale markers are 8 μm in (A), 5 μm in (B), 20 μm in (C) and (E) and 10 μm in (D) and (F).

Table 1
Young's modulus, tensile strength and elongation at break for BCNW and BCNW–PEG films and the various coated systems.

	E (GPa)	Tensile strength (MPa)	ε_b (%)
BCNW	[b] 7.88 ± 0.12	[ab] 74.55 ± 11.48	[a] 1.04 ± 0.13
BCNW–PLA	[b] 7.64 ± 1.20	[ab] 74.93 ± 32.77	[a] 1.07 ± 0.38
BCNW–VTMS	[b] 7.49 ± 0.81	[ab] 62.50 ± 9.06	[a] 0.96 ± 0.13
BCNW–APTS	[ab] 5.55 ± 0.52	[ab] 51.44 ± 5.34	[a] 1.62 ± 0.91
BCNW–PEG	[a] 2.43 ± 0.67	[a] 11.62 ± 2.83	[a] 0.66 ± 0.00
BCNW–PEG–PLA	[ab] 5.10 ± 2.45	[b] 88.87 ± 29.39	[a] 1.56 ± 0.00
Film PLA (Martínez-Sanz et al., 2012d)	1.85 ± 0.08	53.77 ± 1.18	4.93 ± 0.45
MFC film (Plackett et al., 2010)	2.1 ± 0.1	39.0 ± 8.0	2.8 ± 0.9
MFC carboxymethylated film (Siró et al., 2011)	4.4–7.4	182.2–280.7	3.9–12.7

The a and b letters correspond to the ANOVA statistical analysis and Tukey test of the data that indicate that with a 95% confidence level, the values are significantly different.

aim of increasing the ductility of the films, PEG was incorporated into the system. However, it may be observed that its incorporation did not significantly increase the ductility of the material, i.e. the elongation at break, but it led to a reduction in the Young's modulus. According to SEM observations, this effect could be related to the fact that there was a certain phase separation between the crystalline BCNW and the PEG domains.

Barrier properties of both pure BCNW and BCNW–PEG films are displayed in Table 2. The water permeability values were similar to that previously reported for microfibrillated cellulose films (Rodionova et al., 2011), whereas the oxygen permeability measured at 0%RH was between one and two orders lower than the values reported for microfibrillated cellulose (MFC) films (Minelli et al., 2010; Rodionova et al., 2011). This has never been reported before and indicates that BCNW can form more tightly packed films than MFC. The improved barrier properties of the BCNW films may thus be explained by the more compacted structures generated by the vacuum filtration process here applied and by the higher crystallinity of the material as compared to conventional solvent cast microfibrillated cellulose.

Nevertheless, when exposing these materials to high relative humidity conditions, the oxygen permeability dramatically increased. A previous work, in which the oxygen permeability of MFC films was studied at various relative humidities, showed a sharp increase in the oxygen permeability of the films at a relative humidity greater than 70%RH (Aulin et al., 2010). This behaviour is typical of hydrophilic materials, and it was ascribed to the plasticization effect caused by water adsorbed in the surface of the amorphous MFC domains. Water molecules may disrupt hydrogen bonding hence limiting nanofibril–nanofibril interactions and, thus, resulting in an increased mobility of oxygen molecules within the cellulose network.

In addition, when incorporating PEG into the films, higher values for both the water and oxygen permeability were detected. The reason for incorporating PEG into the films was to reduce the rigidity of the films, but, as observed, this plasticization effect was not achieved for the PEG loading here tested and additionally, the material possessed greater water sensitivity. Therefore, the addition of such concentration of PEG did not present any clear advantage.

To summarize, BCNW films presented a homogeneous and compact morphology with excellent barrier properties for low relative humidity, whereas due to their hydrophilic character, at high relative humidity (80%), a considerable increase in the oxygen permeability was observed. The addition of PEG slightly distorted the highly packed structure of the BCNW films, reducing their mechanical performance and increasing their sensitivity to water, thus resulting in a drop in the barrier properties.

3.2. Optical, morphological, chemical and mechanical characterization of the coated systems

As it has been shown in the previous section, the developed BCNW films presented an excellent barrier to oxygen at low relative humidity. Nevertheless, the major problem of these materials was

Table 2
Barrier properties of BCNW and BCNW–PEG films and of the various coated systems. The water permeability and water uptake were measured at 75%RH and the estimated oxygen diffusion and permeability coefficients were measured at 0%RH and 80%RH. Some literature values from MFC films are also included for comparison purposes.

	P·H_2O (kg m/s m^2 Pa) ($\times 10^{-14}$)	Water uptake (%)	D (m^2/s) ($\times 10^{-12}$)	P O_2 0%RH (m^3 m/m^2 s Pa)	P O_2 80%RH (m^3 m/m^2 s Pa)
BCNW	3.55 ± 1.11	4.95 ± 0.74	1.54	6.99×10^{-22}	5.97×10^{-18}
BCNW–PLA	1.19 ± 0.48	4.00 ± 0.47	1.25	–	0.20×10^{-18}
BCNW–VTMS	3.28 ± 1.18	4.66 ± 0.17	1.70	–	5.51×10^{-18}
BCNW–APTS	1.86 ± 0.33	14.41 ± 1.28	0.47	–	1.56×10^{-18}
BCNW–PEG	4.81 ± 1.18	3.40 ± 0.15	3.78	4.06×10^{-22}	7.17×10^{-18}
BCNW-PEG–PLA	1.46 ± 0.53	4.11 ± 0.11	0.95	–	1.83×10^{-18}
Film PLA (Martínez-Sanz et al., 2012d)	1.31 ± 0.01*	0.95 ± 0.15*	3.63	–	1.78×10^{-18}
MFC film literature values	3.81 (Rodionova et al., 2011)	–	–	$6.67 \pm 2.20 \times 10^{-21}$ (Minelli et al., 2010) 2.01×10^{-20} (Rodionova et al., 2011)	2.20×10^{-17} (Minelli et al., 2010) $4.26–5.83 \times 10^{-20}$ (Syverud & Stenius, 2009)** $1.82 \pm 0.11 \times 10^{-21}$ (Plackett et al., 2010)**
MFC carboxymethylated film literature values	–	–	–	–	$4.23–5.71 \times 10^{-21}$ (Siró et al., 2011)** 9.84×10^{-21} (Aulin et al., 2010)**

* Measured at 100%RH.
** Measured at 50%RH.

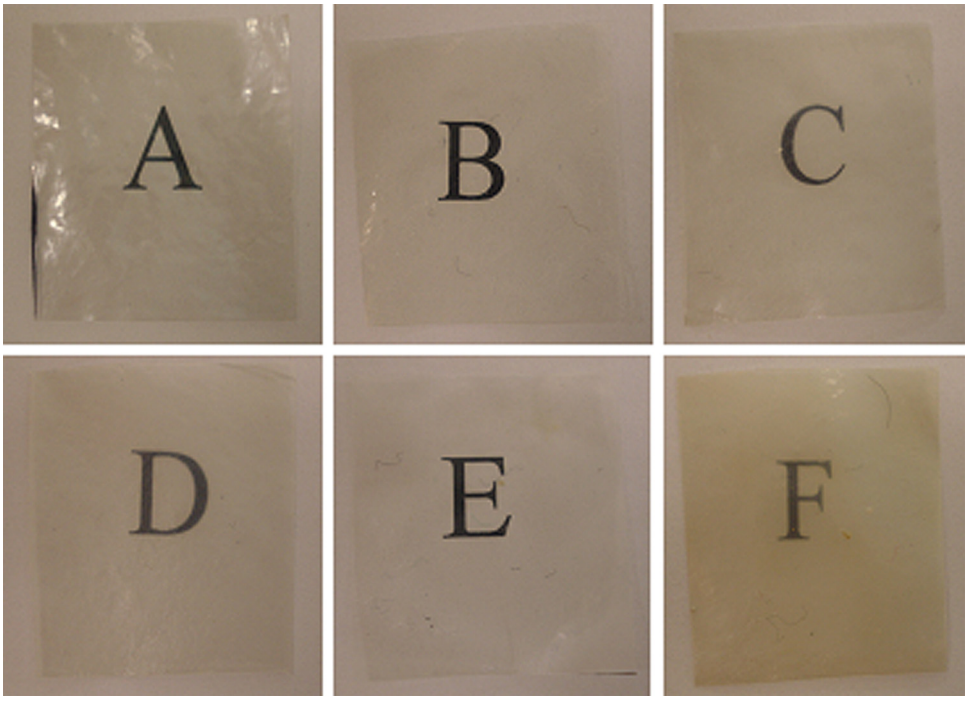

Fig. 2. Photographs of BCNW films: (A) Pure BCNW; (B) BCNW film coated with annealed PLA electrospun nanostructured fibres; (C) BCNW film coated with VTMS; (D) BCNW film coated with APTS; (E) BCNW–PEG film; and (F) BCNW–PEG film coated with annealed PLA electrospun nanostructured fibres.

their high hydrophilicity which makes them very sensitive to water activity, hence reducing drastically the oxygen barrier properties for relative humidities higher than 70%.

With the aim of preserving the low oxygen permeability of the material even at high relative humidity, coating of BCNW with hydrophobic materials was suggested as a feasible route to protect the material from moisture. Nevertheless, the low compatibility of BCNW with hydrophobic materials prevented the use of casting methods to develop multilayer systems or to combine the BCNW with hydrophobic layers through compression moulding, since adhesion between the different layers was very poor and partial or even a complete delamination between the different layers took place (see Figs. S2A and S2B in the Supporting information).

A novel strategy was proposed to overcome this issue and to get uniform layers protecting the BCNW films, involving the use of the electrospinning technique followed by annealing to produce hydrophobic coatings based on PLA. Electrospun PLA fibres were produced by following the optimized procedure described elsewhere (Martínez-Sanz, Lopez-Rubio, & Lagaron, 2012a). These fibres, which presented a uniform morphology (cf. Fig. S3 in the Supporting information), were directly electrospun onto the surface of BCNW and BCNW–PEG films. Subsequently, the coated systems were annealed to temperatures close to the melting point of PLA electrospun fibres, turning the materials nearly transparent (cf. Fig. 2B and F). It is worth mentioning that the film containing PEG presented a slight yellowish colour, which may be indicating that the material underwent partial thermal degradation. This can be explained by the fact that the film containing PEG had an onset degradation temperature close to the annealing temperature applied to the material, just as pointed out by TGA analyses. As observed in Fig. 1C and D, after heating the coated system, a relatively homogeneous PLA layer was formed on both sides of the BCNW film. The average thickness of the PLA fibres layer was ca. 5 μm for both BCNW and BCNW-PEG coated films. It is also interesting to note that the adhesion between the PLA the BCNW layers was very good and no delamination occurred even after cryo-fracturation of the material, just as shown in Fig. 1C and D. These results highlight the convenience of the electrospinning processing technique as an efficient strategy for coating BCNW films, since it provides an enhanced adhesion between the hydrophilic inner layer and the hydrophobic outer layers without the need for adhesive layers.

Besides being homogeneously distributed, the applied PLA coatings were continuous and hence, as observed in Fig. 3, the typical spectrum of PLA was obtained when analyzing the coated system surface by ATR-FT-IR. From these spectra it can be observed that the broad band located between 3000 and 3700 cm^{-1}, corresponding to OH stretching intramolecular hydrogen bonds (Carrillo, Colom, Suñol, & Saurina, 2004), characteristic of hydrophilic materials, completely disappeared after coating with PLA. Therefore, the last annealing step resulted in efficient nanofiber coalescence and substrate adherence promotion for the

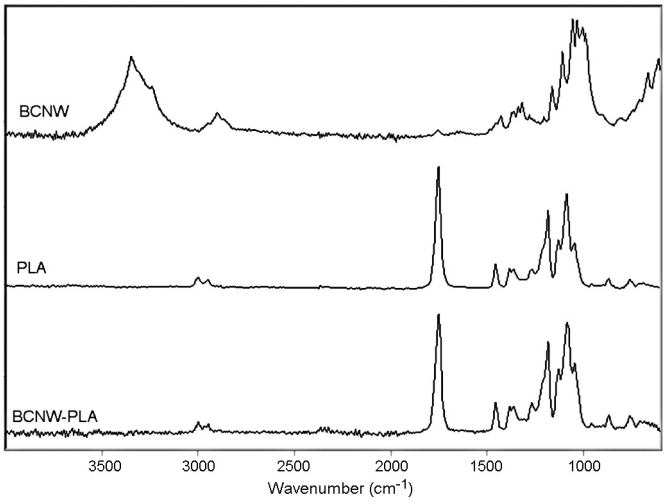

Fig. 3. ATR-FT-IR spectra of BCNW film, PLA electrospun fibres and BCNW coated with annealed PLA electrospun nanostructured fibres.

discontinuous electrospun fibres deposited onto the BCNW films into a compacted and continuous PLA layer.

To evaluate the efficiency of the coating method based on electrospinning followed by annealing, a second approach already described in the literature was suggested for protecting the BCNW films from moisture. This method consisted in coating with thin layers of silanes, which are thought to react with the hydroxyl groups present in the surface of cellulose and form layers with different functionalities (Daniel, 1999; Lee & Kim, 2012; Luechinger, Prins, & Pirngruber, 2005; Tingaut, Hauert, & Zimmermann, 2011). In this work two different silanes, i.e. (3-aminopropyl)trimethoxysilane (APTS) and vinyltrimethoxysilane (VTMS), both allowed for food-contact applications, were used for coating BCNW films. The morphology of cryo-fractured sections of silane-coated BCNW films is shown in Fig. 1E and F. Despite the fact that both silanes were applied by following the same procedure, the average thickness of the coating was different in each case. For the APTS, the outer layer presented an average thickness of 9 μm whereas for the VTMS, the average thickness was 0.8 μm. The adhesion between the silane and the BCNW layers seemed to be good in both cases, although, probably due to the different thickness of the coatings, it was easier to identify the interface between both materials for the APTS coated system. As observed in Fig. 2C and D, the films prepared by coating with silanes preserved a good contact transparency, although it was slightly diminished when compared to the pure BCNW film.

Fig. 4A and B shows the mechanism proposed for the reaction between silanes and cellulose based on previous works (Lee & Kim, 2012). In the presence of moisture, the methoxy groups from the silanes tend to be replaced by hydroxyl groups, thus forming silanols. Hydroxyl groups from cellulose and silanol react and the silanol groups bond to the cellulose chain without modification of its functional group (amino or vinyl). In the case of APTS, amino functional groups can further react with hydroxyl groups from silanols and, therefore, additional layers can be created via hydrogen bonding. This is probably the reason why the thickness of the outer layer was greater for APTS than for VTMS. During the final curing step, the number of hydroxyl groups from silanols is reduced by cross-linking (Angst & Simmons, 1991).

In order to further study the interactions established between BCNW and the silanes, ATR–FTIR analyses of pure BCNW films, silanes and silane-coated BCNW films were carried out and the recorded spectra are displayed in Fig. 5. The spectrum of BCNW–APTS was different to that of pure BCNW or pure APTS, suggesting that the cellulose hydroxyl groups effectively reacted with some chemical groups from the silane. The spectra from both pure APTS and from the BCNW–APTS films displayed several peaks characteristic from amino groups, such as the band located at 2939 cm^{-1} which corresponds to N–H stretching, the peak appearing at 1189 cm^{-1} which is assigned to C–N stretching and the band at 810 cm^{-1} which corresponds to N–H wagging. From the spectra it is also worth noting that a decrease in the intensity of the band located at 2840 cm^{-1}, characteristic from Si–O–CH_3 (Lee & Kim, 2012), was observed and a band characteristic from Si–O–C (Lee & Kim, 2012), located at approximately 1000 cm^{-1}, was discerned after reaction of APTS with cellulose. Additionally, the broad band between 3000 and 3700 cm^{-1} detected for the coated material, can be assigned to NH_2 stretching and to Si–OH and the peaks at 1635 cm^{-1} and 1568 cm^{-1} to NH_2 stretching vibration and to the bending band of protonated amines, respectively (Xia

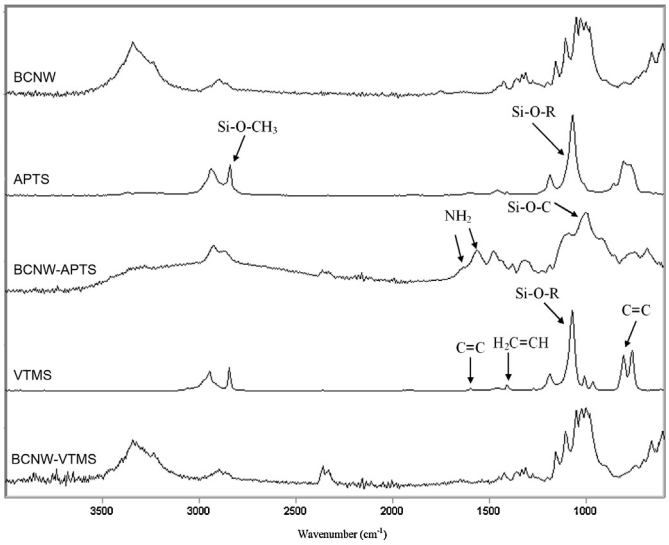

Fig. 5. ATR-FTIR spectra of BCNW films and BCNW coated with APTS and VTMS.

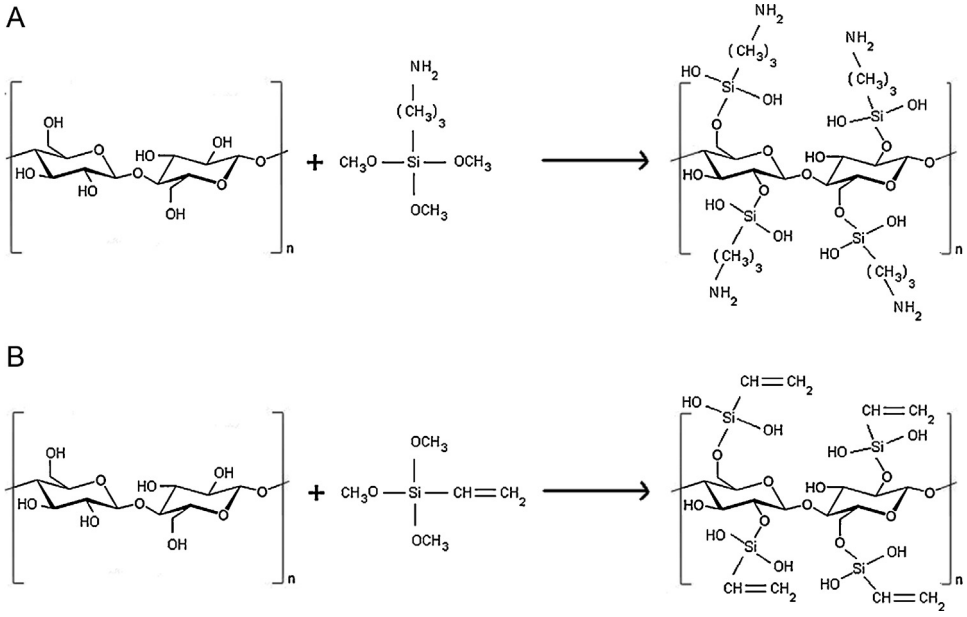

Fig. 4. Proposed mechanism for the reaction of BCNW with APTS (A) and with VTMS (B).

et al., 2006). These spectral changes confirmed that indeed methoxy groups from the silane were hydrolyzed and the silane was bonded to cellulose. On the other hand, the presence of Si–OH bonds suggests that the curing process to which the films were subjected was not sufficient for completely removing hydroxyl groups through cross-linking.

The spectrum for VTMS was characterized by the major bands appearing at 1075 cm^{-1}, 810 cm^{-1} and 764 cm^{-1}, corresponding to Si–O–R bonds (Velamakanni et al., 2010), C=C stretching (Xie, Wang, Zhao, Wei, & Sun, 2010) and C–H out of plane deformation (Rosa et al., 2010), respectively. In addition, two other bands characteristic from the vinyl functional group can be detected at 1410 cm^{-1}, corresponding to CH deformation vibration in H_2C=CH group (Xie et al., 2010) and at 1600 cm^{-1}, assigned to C=C stretching (Xie et al., 2010). No significant spectral changes were observed after coating the BCNW layer with VTMS, although a detailed examination allowed distinguishing the band for the vinyl functional group, at ca. 1410 cm^{-1}. In addition, the intensity of the broad band between 3000 and 3600 cm^{-1} corresponding to OH stretching intramolecular bonds in cellulose was decreased but not to a great extent since Si–OH groups also present a characteristic band in this region. The reason for not detecting major VTMS peaks in the ATR-FT-IR spectrum of the coated system may be due to the fact that the outer layer of VTMS was too thin and, thus, the ATR signal was predominantly coming from the inner layer. Therefore, from ATR-FT-IR analyses it seems that the amino groups from APTS were much more reactive than vinyl groups from VTMS and as a result, the layers of silane chains were more easily formed for the APTS, through the interaction of amino groups with silanol groups.

Regarding the mechanical properties of the coated films, as observed in Table 1, none of the applied coatings seemed to strongly affect the mechanical performance of the neat BCNW and BCNW–PEG films. When the BCNW–PEG film was coated with annealed PLA electrospun nanostructured fibres, the system presented a slightly higher Young's modulus, tensile strength and elongation at break, suggesting that the outer PLA layer might be improving the mechanical performance of the inner layer, probably protecting it from the detrimental effect of moisture and/or PEG migration. The only case in which coating presented a slight unfavourable effect on the mechanical properties corresponded to coating with APTS. In that case, the Young's modulus and tensile strength of the material slightly decreased, although this effect was not statistically significant.

3.3. Barrier properties of the coated systems

The main purpose of this work was to improve the barrier of BCNW at high relative humidity by combining them with outer layers of materials less sensitive to moisture. In order to confirm that this objective was achieved and to select the coated system, which showed the higher barrier properties, both water and oxygen permeability of the developed materials were evaluated.

Table 2 gathers water permeability and water uptake values as well as the estimated diffusion coefficients for the developed films. From the results it is observed that BCNW films presented lower water barrier than a PLA film. Similar permeability values have been reported for microfibrillated cellulose films (Rodionova et al., 2011). On the other hand, when coating BCNW or BCNW-PEG films with annealed PLA electrospun nanostructured fibres, water permeability dropped by ca. 66% and 70%, respectively, thus providing the greatest water barrier from all the developed materials. For the silane-coated materials, APTS was able to reduce water permeability by ca. 48% whereas a slight drop of ca. 8% was seen for VTMS-coated films.

The strategy usually applied for improving cellulose barrier properties for high water activities is to modify the surface by introducing hydrophobic functional groups through reaction with the cellulose hydroxyl groups. For example, by acetylating MFC it was possible to decrease water permeability up to 22% with respect to the unmodified MFC film (Rodionova et al., 2011). Nevertheless, from the results obtained through this work it is observed that coating with annealed PLA electrospun nanostructured fibres reduces water permeability more effectively than surface modification of cellulose, resulting in systems with greater water barrier than that of previously reported materials. It is worth noting that the reduction in water permeability attained for annealed PLA electrospun nanostructured fibres coated films was due to a combination of reduced sorption and diffusion. From Table 2 it is also observed that PLA films presented lower sorption but greater diffusion than BCNW films. Therefore, in the coated system the PLA outer layer limited water sorption due to the specific PLA chemistry, whereas the inner BCNW layer provided a highly crystalline and compacted structure, which limited water diffusion through the system.

A relatively low water sorption was observed for BCNW and BCNW–PEG films. The water uptake value obtained for the BCNW film was significantly lower than that previously estimated for MFC films and sisal whisker films produced by solution casting (Aulin et al., 2010; Belbekhouche et al., 2011). Probably due to the very high crystallinity of BCNW there were limited amorphous domains available for water sorption as compared to less crystalline materials. The incorporation of PEG reduced the water uptake since hydroxyl groups from PEG interacted with those from cellulose via hydrogen bonding, hence limiting the amount of free hydroxyl groups available for water sorption. Nevertheless, the negative effect of PEG on the morphology of films, which had a less compacted structure (cf. Fig. 1B), resulted in higher diffusion through the system.

When coating BCNW with APTS the sorption was significantly increased, thus confirming that amino and silanol groups were present in the material, just as suggested by the mechanism shown in Fig. 4A. However, water molecules remained bonded to silanol and amino groups from the outer coating layer, hence reducing the free volume at the surface and limiting the diffusion to the underneath BCNW film. Previous studies on moisture sorption of organosiloxane layers showed that even though the outer layer was highly hydrophobic, the moisture sorption of silicon dioxide silanized surfaces was greater than for the unsilanized surfaces due to the presence of silanol groups as a result of typically incomplete curing. By more extensive curing of the silanol coating, cross-linking was promoted and, thus, the number of silanol groups acting as sorption sites was reduced (Angst & Simmons, 1991). Further sorption and desorption analyses (results not shown) showed that for the sorption process, the uncoated BCNW film reached the equilibrium faster than the APTS coated system. On the contrary, for the desorption process, the coated system released considerably faster the sorbed water and reached the equilibrium. This result suggests that, in the presence of moisture, hydrogen bonds established between hydroxyl groups in the APTS coating are disrupted after the curing process; hence, water is primarily sorbed by free hydroxyl groups.

Contact angle measurements were additionally carried out to investigate the effect of the applied outer layers on the surface water affinity and results are listed in Table 3. High contact angle values, ranging from 70° to 90°, are characteristic from hydrophobic surfaces such as silicone or fluorocarbon polymers, while low contact angle values, between 0° and 30°, are observed for highly hydrophilic surfaces such as glass or mica (Gilliland, Yokoyama, & Yip, 2005). The contact angle of the BCNW film, which was similar to that reported for MFC films (Rodionova et al., 2011) and TEMPO-oxidized cellulose nanofibres films (Fukuzumi et al., 2009), was characteristic of hydrophilic materials. As shown in Fig. 6, the wettability of films was further increased when incorporating

Table 3
Contact angles measured after 30 s for pure BCNW and BCNW–PEG films and the various coated systems.

	Contact angle (°)
BCNW	[b] 43.8 ± 0.7
BCNW–PLA	[de] 77.8 ± 0.3
BCNW–VTMS	[c] 64.3 ± 1.9
BCNW–APTS	[d] 73.2 ± 1.6
BCNW–PEG	[a] 27.3 ± 2.3
BCNW–PEG–PLA	[e] 79.6 ± 1.6

The a, b, c, d and e letters correspond to the ANOVA statistical analysis and Tukey test of the data that indicate that with a 95% confidence level, the values are significantly different.

PEG into the system, as a consequence of the hydrophilic character of PEG and the increased roughness of the material, which is known to decrease contact angles for hydrophilic materials (Chau, Bruckard, Koh, & Nguyen, 2009). On the contrary, as observed in Fig. 6 and Table 3, the systems coated by annealed PLA electrospun nanostructured fibres or APTS showed significantly higher contact angles of ca. 70–80°. As a reference, contact angles of up to 82.7°, 94° and 146° have been reported for films from acetylated MFC (Rodionova et al., 2011), TEMPO-oxidized cellulose nanofibers treated with alkylketene dimer (Fukuzumi et al., 2009) and MFC surface treated with chlorodimethyl isopropylsilane (Andresen et al., 2006), respectively, although all of these mentioned works involved chemical modification of the cellulosic material.

As indicated by the measured water contact angles, coating of BCNW with annealed PLA electrospun nanostructured fibres or APTS resulted in hydrophobic surfaces. It should be noted that whereas PLA-coated films presented decreased water uptake, APTS-coated films presented the greatest water sorption value for the films tested. In terms of chemical composition, the APTS coating contained amino and hydroxyl groups which were responsible for water sorption, but these groups were partially cross-linked after the curing step and apparently they tended to remain in the inner side of the coating layer, whereas the surface of the coating seemed to be composed of the hydrophobic alcoxysilane regions. Another fact to take into account is that water contact angle measurements are typically carried out immediately after deposition of the water droplet. We observed that 1 h after deposition of the droplet, water completely expanded over the film surface. Therefore, in agreement with water permeability and sorption experiments, it seems that although the surface of the APTS layer showed, in principle, a hydrophobic behaviour, this layer possessed hydroxyl and amino groups which interacted via hydrogen bonding with water and, thus became hydrophilic upon contact. On the other hand, upon removal of moisture contact, the film recovered its original hydrophobic behaviour.

It has already been discussed that BCNW films present excellent oxygen barrier at low relative humidity, but their high moisture sensitivity results in dramatically decreased barrier when the relative humidity is higher than 70% (Aulin et al., 2010). Table 2 displays the oxygen permeability values for the developed materials at 80%RH, i.e. within the range in which the oxygen permeability of the BCNW films was dramatically increased, to a point where the material became highly permeable. This strong water sensitivity can limit the usability of cellulosic materials in many applications, as it can compromise barrier properties. From the results, it is observed that the greatest oxygen barrier was attained when coating BCNW films with annealed PLA electrospun nanostructured fibres. Using this method, it was possible to reduce the oxygen permeability by ca. 97% and 74% with respect to the BCNW and BCNW–PEG films, respectively at 80% RH. In agreement with water permeability results, it seems that the outer PLA layer limited the amount of water that reached the inner BCNW layer and, therefore, the oxygen permeability was kept low with increasing water activity.

In the case of the BCNW films coated with silanes it is worth noting that a 74% reduction in the oxygen permeability was observed when the BCNW film was coated with APTS, whereas coating with

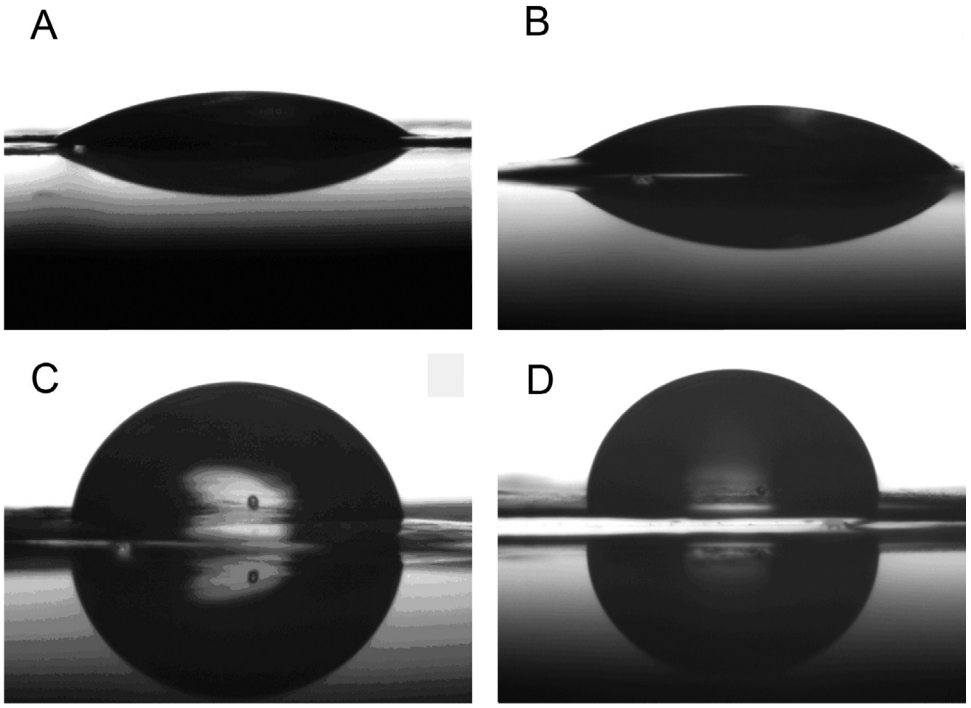

Fig. 6. Images of water droplet in contact angle measurements for BCNW film (A), BCNW-PEG film (B), BCNW coated with annealed PLA electrospun nanostructured fibres (C) and BCNW coated with APTS (D).

VTMS only caused a ca. 8% reduction. This again was related to the water permeability of the materials, which was significantly lower for APTS. Even though water sorption was high for APTS-coated systems, it seems that water molecules remained adsorbed in the outer coating layer and did not significantly penetrate and plasticize the inner BCNW layer.

As observed from Table 2, most oxygen permeability values previously reported for MFC films were measured at 50%RH and were reported to be two or three orders of magnitude higher barrier than the ones reported here at 80%RH. Nevertheless, it should be taken into account that oxygen permeability of cellulosic films is strongly altered by moisture. For example, when increasing the relative humidity from 0% to 50%, the oxygen permeability increases by three orders of magnitude (Kvien et al., 2007). This effect in gas barrier drop is even more evident when increasing the water activity over 70%RH (Kvien et al., 2007). In fact, the oxygen permeability of the developed BCNW films was significantly lower than that reported for MFC at 80%RH in a previous work (Petersson & Oksman, 2006), once again confirming the extremely highly crystalline and packed structure of BCNW as compared to MFC.

4. Conclusions

In the present work, films from highly crystalline BCNW were prepared by vacuum filtration of aqueous suspensions. These films presented a highly compacted structure of nanofibrils' layers, a relatively good thermal stability and excellent barrier to oxygen at low relative humidity. However, the permeability dramatically increased at 80%RH due to the disruption of the strong nanocrystals network held by hydrogen bonding between hydroxyl groups from cellulose. The incorporation of PEG resulted in a more heterogeneous structure, with reduced mechanical performance and increased water sensitivity.

A novel approach, involving the coating of the BCNW film by electrospun PLA fibres homogenized by annealing, was developed to protect the BCNW film from moisture. Through this process it was possible to create a uniform and continuous PLA layer which presented a good adhesion with the BCNW layer. A drop of ca. 70% was estimated for water permeability, which was attributed mainly to reduced water sorption. Additionally, it was possible to limit the effect of moisture on the oxygen permeability and hence, reductions of up to 97% were detected for the oxygen permeability at 80%RH. Water contact angles increased up to ca. 80°, thus confirming that by this method the hydrophilic surface of the BCNW film was turned into a hydrophobic surface. To evaluate the efficiency of this innovative coating strategy, a second method consisting in the application of silanes outer layers with amino (APTS) and vinyl (VTMS) functional groups was also developed and the results were compared. APTS was seen to generate more hydrophobic surfaces than VTMS, with a water contact angle of 73°, and enhanced the barrier properties of the coated systems more efficiently, providing a decrease of 48% in water permeability and a 74% decrease in the oxygen permeability at 80%RH.

This work has demonstrated that it is possible to produce cellulose-based biomaterials with high barrier to oxygen across relative humidity and also to water vapour by combining an inner layer of a highly crystalline material such as BCNW with outer layers that promote a more hydrophobic behaviour for the overall structure. The use of the electrospinning technique is critical to guarantee a good adhesion between the inner and the outer layers. This enhanced adhesion is one of the key factors for the improved barrier properties attained, which are even better than those attained for other conventional strategies such as coating with hydrophobic silanes.

Acknowledgements

M. Martínez-Sanz would like to thank the Spanish Ministry of Education for the FPU grant 1484. A. Lopez-Rubio is the recipient of a "Ramon y Cajal" contract from the Spanish Ministry of Science and Innovation. The authors acknowledge financial support from MICINN (MAT2009-14533-C02-01 project and MAT2012-38947-C02-01) and the EU FP7 ECOBIOCAP project. M.J. Fabra is acknowledged for carrying out the contact angle measurements. Dr. Luis Cabedo, from Universitat Jaume I, is acknowledged for his support with mechanical testing. The Electronic Microscopy department in the SCIE from the University of Valencia is acknowledged for the support with SEM and TEM analyses.

Appendix A. Supplementary data

Supplementary data associated with this article can be found, in the online version, at http://dx.doi.org/10.1016/j.carbpol.2013.07.020.

References

Andresen, M., Johansson, L. S., Tanem, B. S., & Stenius, P. (2006). Properties and characterization of hydrophobized microfibrillated cellulose. *Cellulose*, *13*(6), 665–677.

Angst, D. L., & Simmons, G. W. (1991). Moisture absorption characteristics of organosiloxane self-assembled monolayers. *Langmuir*, *7*(10), 2236–2242.

Aulin, C., Gällstedt, M., & Lindström, T. (2010). Oxygen and oil barrier properties of microfibrillated cellulose films and coatings. *Cellulose*, *17*(3), 559–574.

Belbekhouche, S., Bras, J., Siqueira, G., Chappey, C., Lebrun, L., Khelifi, B., Marais, S., & Dufresne, A. (2011). Water sorption behavior and gas barrier properties of cellulose whiskers and microfibrils films. *Carbohyd. Polym.*, *83*(4), 1740–1748.

Carrillo, F., Colom, X., Suñol, J. J., & Saurina, J. (2004). Structural FTIR analysis and thermal characterisation of lyocell and viscose-type fibres. *Eur. Polym. J.*, *40*(9), 2229–2234.

Chau, T. T., Bruckard, W. J., Koh, P. T. L., & Nguyen, A. V. (2009). A review of factors that affect contact angle and implications for flotation practice. *Adv. Colloid Interface*, *150*(2), 106–115.

Daniel, B. (1999). Functionalized micelle-templated silicas (MTS) and their use as catalysts for fine chemicals. *Microporous Mesoporous Mater.*, *27*(2-3), 329–344.

De Souza Lima, M. M., & Borsali, R. (2004). Rodlike cellulose microcrystals: structure, properties, and applications. *Macromol. Rapid Commun.*, *25*(7), 771–787.

Fukuzumi, H., Saito, T., Iwata, T., Kumamoto, Y., & Isogai, A. (2009). Transparent and high gas barrier films of cellulose nanofibers prepared by TEMPO-mediated oxidation. *Biomacromolecules*, *10*(1), 162–165.

Gilliland, J. W., Yokoyama, K., & Yip, W. T. (2005). Comparative study of guest charge–charge interactions within silica sol–gel. *J. Phys. Chem. B*, *109*(11), 4816–4823.

Hirai, A., Inui, O., Horii, F., & Tsuji, M. (2009). Phase separation behavior in aqueous suspensions of bacterial cellulose nanocrystals prepared by sulfuric acid treatment. *Langmuir*, *25*(1), 497–502.

Iguchi, M., Yamanaka, S., & Budhiono, A. (2000). Bacterial cellulose—a masterpiece of nature's arts. *J. Mater. Sci.*, *35*(2), 261–270.

Kvien, I., Sugiyama, J., Votrubec, M., & Oksman, K. (2007). Characterization of starch based nanocomposites. *J. Mater. Sci.*, *42*(19), 8163–8171.

Lee, S. J., & Kim, B. K. (2012). Covalent incorporation of starch derivative into waterborne polyurethane for biodegradability. *Carbohyd. Polym.*, *87*(2), 1803–1809.

Luechinger, M., Prins, R., & Pirngruber, G. D. (2005). Functionalization of silica surfaces with mixtures of 3-aminopropyl and methyl groups. *Microporous Mesoporous Mater.*, *85*(1-2), 111–118.

Martínez-Sanz, M., Lopez-Rubio, A., & Lagaron, J. M. (2011). Optimization of the nanofabrication by acid hydrolysis of bacterial cellulose nanowhiskers. *Carbohyd. Polym.*, *85*(1), 228–236.

Martínez-Sanz, M., Lopez-Rubio, A., & Lagaron, J. M. (2012a). Dispersing bacterial cellulose nanowhiskers in polylactides via electrohydrodynamic processing. *J. Polym. Environ.*, under review

Martínez-Sanz, M., Lopez-Rubio, A., & Lagaron, J. M. (2012b). Nanocomposites of ethylene vinyl alcohol copolymer with thermally resistant cellulose nanowhiskers by melt compounding (I): morphology and thermal properties. *J. Appl. Polym. Sci.*, http://dx.doi.org/10.1002/app.38433, in press

Martínez-Sanz, M., Lopez-Rubio, A., & Lagaron, J. M. (2012c). Nanocomposites of ethylene vinyl alcohol copolymer with thermally resistant cellulose nanowhiskers by melt compounding (II): water barrier and mechanical properties. *J. Appl. Polym. Sci.*, http://dx.doi.org/10.1002/app.38432, in press

Martínez-Sanz, M., Lopez-Rubio, A., & Lagaron, J. M. (2012d). Optimization of the dispersion of unmodified bacterial cellulose nanowhiskers into polylactide via melt compounding to significantly enhance barrier and mechanical properties. *Biomacromolecules*, *13*(11), 3887–3899.

Martínez-Sanz, M., Olsson, R. T., Lopez-Rubio, A., & Lagaron, J. M. (2011). Development of electrospun EVOH fibres reinforced with bacterial cellulose nanowhiskers. Part I: Characterization and method optimization. *Cellulose*, *18*(2), 335–347.

Minelli, M., Baschetti, M. G., Doghieri, F., Ankerfors, M., Lindström, T., Siró, I., & Plackett, D. (2010). Investigation of mass transport properties of microfibrillated cellulose (MFC) films. *J. Membr. Sci.*, *358*(1-2), 67–75.

Petersson, L., Kvien, I., & Oksman, K. (2007). Structure and thermal properties of poly(lactic acid)/cellulose whiskers nanocomposite materials. *Compos. Sci Technol.*, *67*(11-12), 2535–2544.

Petersson, L., & Oksman, K. (2006). Biopolymer based nanocomposites: comparing layered silicates and microcrystalline cellulose as nanoreinforcement. *Compos. Sci. Technol.*, *66*(13), 2187–2196.

Plackett, D., Anturi, H., Hedenqvist, M., Ankerfors, M., Gällstedt, M., Lindström, T., & Siró, I. (2010). Physical properties and morphology of films prepared from microfibrillated cellulose and microfibrillated cellulose in combination with amylopectin. *J. Appl. Polym. Sci.*, *117*(6), 3601–3609.

Rånby, B. G. (1949). Aqueous colloidal solutions of cellulose micelles. *Acta Chem. Scand.*, *3*, 649–650.

Rodionova, G., Lenes, M., Eriksen, Ø., & Gregersen, Ø. (2011). Surface chemical modification of microfibrillated cellulose: improvement of barrier properties for packaging applications. *Cellulose*, *18*(1), 127–134.

Rosa, M. F., Medeiros, E. S., Malmonge, J. A., Gregorski, K. S., Wood, D. F., Mattoso, L. H. C., Glenn, G., Orts, W. J., & Imam, S. H. (2010). Cellulose nanowhiskers from coconut husk fibers: effect of preparation conditions on their thermal and morphological behavior. *Carbohyd. Polym.*, *81*(1), 83–92.

Siró, I., Plackett, D., Hedenqvist, M., Ankerfors, M., & Lindström, T. (2011). Highly transparent films from carboxymethylated microfibrillated cellulose: the effect of multiple homogenization steps on key properties. *J. Appl. Polym. Sci.*, *119*(5), 2652–2660.

Syverud, K., & Stenius, P. (2009). Strength and barrier properties of MFC films. *Cellulose*, *16*(1), 75–85.

Ten, E., Turtle, J., Bahr, D., Jiang, L., & Wolcott, M. (2010). Thermal and mechanical properties of poly(3-hydroxybutyrate-co-3-hydroxyvalerate)/cellulose nanowhiskers composites. *Polymer*, *51*(12), 2652–2660.

Tingaut, P., Hauert, R., & Zimmermann, T. (2011). Highly efficient and straightforward functionalization of cellulose films with thiolene click chemistry. *J. Mater. Chem.*, *21*(40), 16066–16076.

Velamakanni, A., Blackwell, D. L., Yang, D., Sonawane, S., Addagulla, S., & Major, J. S. (2010). Synthesis and characterization of functionalized silane-based copolymers for thermally robust polymer-silica hybrids. *Polym. Chem.*, *1*(6), 916–921.

Wan, Y. Z., Huang, Y., Yuan, C. D., Raman, S., Zhu, Y., Jiang, H. J., He, F., & Gao, C. (2007). Biomimetic synthesis of hydroxyapatite/bacterial cellulose nanocomposites for biomedical applications. *Mater. Sci. Eng., C*, *27*(4), 855–864.

Xia, B., Xiao, S.-J., Guo, D.-J., Wang, J., Chao, J., Liu, H.-B., Pei, J., Chen, Y.-Q., Tang, Y.-C., & Liu, J.-N. (2006). Biofunctionalisation of porous silicon (PS) surfaces by using homobifunctional cross-linkers. *J. Mater. Chem.*, *16*(6).

Xie, Z., Wang, F., Zhao, N., Wei, W., & Sun, Y. (2010). Hydrophobisation of activated carbon fiber and the influence on the adsorption selectivity towards carbon disulfide. *Appl. Surf. Sci.*, *257*(8), 3596–3602.